

# The old open cluster NGC 2112: updated estimates of fundamental parameters based on a membership analysis<sup>\*</sup> †

G. Carraro<sup>1,2,3,4</sup>, S. Villanova<sup>2,5</sup>, P. Demarque<sup>4</sup>, C. Moni Bidin<sup>3</sup>, and M.V. McSwain<sup>4,6</sup> ‡

<sup>1</sup>ESO, Casilla 19001, Santiago 19, Chile

<sup>2</sup>Dipartimento di Astronomia, Università di Padova, vic. Osservatorio 3, Padova, Italy

<sup>3</sup>Departamento de Astronomía, Universidad de Chile, Casilla 36-D, Santiago, Chile

<sup>4</sup>Astronomy Department, Yale University, P.O. Box 208101 New Haven, CT 06520-8101 USA

<sup>5</sup>Departamento de Física, Facultad de Ciencias Físicas y Matemáticas Universidad de Concepción, Casilla 160-C, Concepción, Chile

<sup>6</sup>Department of Physics, Lehigh University, 16 Memorial Drive East, Bethlehem, PA 18015, USA

Accepted 1988 December 15. Received 1988 December 14; in original form 1988 October 11

## ABSTRACT

We report on a new, wide field ( $20' \times 20'$ ), multicolor ( $UBVI$ ), photometric campaign in the area of the nearby old open cluster NGC 2112. At the same time, we provide medium-resolution spectroscopy of 35 (and high-resolution of additional 5) Red Giant and Turn Off stars. This material is analyzed with the aim to update the fundamental parameters of this traditionally difficult cluster, which is very sparse and suffers from heavy field star contamination. Among the 40 stars with spectra, we identified 21 *bona fide* radial velocity members which allow us to put more solid constraints on the cluster's metal abundance, long suggested to be as low as the metallicity of globulars. As indicated earlier by us on a purely photometric basis (Carraro et al. 2002), the cluster  $[\text{Fe}/\text{H}]$  abundance is slightly super-solar ( $[\text{Fe}/\text{H}] = 0.16 \pm 0.03$ ) and close to the Hyades value, as inferred from a detailed abundance analysis of 3 of the 5 stars with higher resolution spectra. Abundance ratios are also marginally super solar.

Based on this result, we revise the properties of NGC 2112 using stellar models from the Padova and Yale-Yonsei groups.

For this metal abundance, we find the cluster's age, reddening, and distance values are 1.8 Gyr, 0.60 mag, and 940 pc, respectively. Both the Yale-Yonsei and Padova models predict the same values for the fundamental parameters within the errors.

Overall, NGC 2112 is a typical solar neighborhood, thin disk star cluster, sharing the same chemical properties of F-G stars and open clusters close to the Sun.

This investigation outlines the importance of a detailed membership analysis in the study of disk star clusters.

**Key words:** Open clusters and associations: general– Open clusters and associations: individual: NGC 2112

## 1 INTRODUCTION

Gathering information on metal abundance and abundance ratios of many Galactic clusters located in different region

of the disk and with different ages is mandatory to study the chemical evolution of the Galactic disk. This, in turn, provides us with hints on the formation mechanism of the disk and its relation with the other major components of the Galaxy, the halo and bulge (Janes & Phelps 1994, Carraro et al. 1998).

However, a frequent, well known problem in the study of open star clusters is the stellar contamination from the general Galactic disk field, which complicates the analysis of the Color Magnitude Diagram (CMD). It also makes it difficult to derive fundamental cluster parameters, especially metallicity, when only a few stars are observed.

A notorious example in this context is the nearby old open cluster NGC 2112 (Collinder 76, C 0551-0031, OCL 509),

<sup>\*</sup> This paper includes data gathered with the 6.5 Magellan Telescopes, located at Las Campanas Observatory, Chile

† The data discussed in this paper will be made available at the WEBDA open cluster database <http://www.univie.ac.at/webda>, which is maintained by E. Paunzen and J.-C. Mermilliod

‡ email: gcarraro@eso.org (GC), sandro.villanova@unipd.it (SV), demarque@astro.yale.edu (PD), mbidin@das.uchile.cl (CMB), mcswain@lehigh.edu (MVM)

which has a reputation of suffering from heavy field star contamination (Brown et al. 1996), and for this reason its basic parameters remain poorly constrained.

The first investigation on NGC 2112 was carried out by Richtler (1985, hereinafter R85), who obtained photographic BV photometry for about 80 stars down to  $V=15$ . Although his photometry barely reaches the cluster Turn-Off (TO), he nevertheless drew attention to this probably old, so far neglected cluster, and he suggested that NGC 2112 has a reddening of  $\sim 0.5$  mag and lies  $\sim 800$  pc from the Sun. By analyzing additional Stromgren photometry, he proposed that the cluster had to be very metal poor ( $[\text{Fe}/\text{H}]$  as low as -1.4). A more accurate and deeper analysis was performed a few years later by Richtler & Kaluzny (1989). They obtained BV CCD photometry for about 500 stars in a field of 200 arcmin<sup>2</sup>. Additionally, they obtained moderate resolution spectra for a handful of bright stars. Their conclusions were that the cluster was very contaminated by field stars. Nevertheless, they were able to strengthen the suggestions of Richtler (1985, hereinafter R85) by confirming that the cluster is indeed old (3-5 Gyrs), is located  $700\div 800$  pc from the Sun and has a reddening of  $E(B-V)=0.60$  mag. Lacking a membership analysis, no further information on the cluster metallicity was provided.

Photometry in the Washington system by Geisler (1987) and Geisler, Claria & Minniti (1991) seems to confirm the previous suggestions that NGC 2112 is very metal poor ( $[\text{Fe}/\text{H}]$  as low as -1.3).

More recently, three spectroscopic campaigns have been carried out in the field of the cluster. Friel & Janes (1993, hereinafter FJ93) present moderate resolution spectra of 6 stars. Out of these, 5 are considered members, and an average  $[Fe/H]$  of  $-0.52\pm 0.21$  has been found. This is significantly larger than all the previous determinations. Brown et al. (1996, hereinafter BWGO96) used the Blanco Echelle on CTIO to obtain high-resolution spectroscopy of 6 stars. They accepted just one star as a definitive member, providing an even higher metal content value,  $[\text{Fe}/\text{H}]=-0.15$ , only slightly lower than the solar value. Finally, Mermilliod & Mayor (2007, hereinafter MM07) enlarged the sample of spectroscopic members to 3, out of 6 stars observed with Coravel. They underlined the need to obtain radial velocities for a larger sample down to  $V \approx 14.5$  to better probe the shape of the Red Giant Branch (RGB). At the same time, this would also provide much firmer metallicity estimates.

In Carraro et al. (2002) we reported a Johnson BVI photometry of the cluster down to magnitude  $V=20$ . Assuming the metal content found by Brown et al. (1996), we found a reddening of  $E(B-V)=0.63\pm 0.14$ , a distance of  $850\pm 100$  pc, and an age of  $2.0\pm 0.3$  Gyr. We argued on a purely photometric basis that the metallicity cannot be much lower than BWGO96 value, and we stressed the need for a new, more detailed spectroscopic investigation of the cluster.

In this paper we attempt such an investigation by securing the deepest and widest field coverage multicolor ( $UBVI$ ) photometry of NGC 2112 to date. At the same time, we provide moderate and high resolution spectroscopy of 40 stars. With these data at hand, we present robust and updated determinations of the cluster's basic properties.

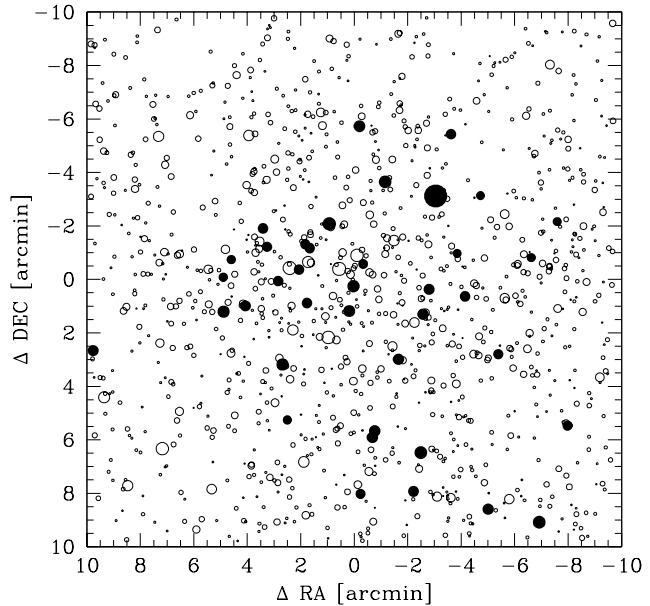


**Figure 1.** V filter map of the field covered by our photometry. Stars (empty circles) are plotted according to their magnitude. North is up and East to the left. The field is 20 arcmin on a side and centered at  $(X,Y) = (2046,2092)$  on star #593, which has  $\alpha = 05:53:43.75$  and  $\delta = +00:23:56.4$ . With filled circles we indicate stars observed spectroscopically.

## 2 OBSERVATIONS AND DATA REDUCTION

In this work we present photometry and spectroscopy in the field of NGC 2112 obtained with three different telescopes. For this reason, the details of data acquisition and reduction are presented in the next three sub-sections.

### 2.1 Photometry

$U, B, V$ , and  $I$  images centered on NGC 2112 were obtained at the Cerro Tololo Inter-American Observatory 1.0 m telescope, which is operated by the SMARTS<sup>1</sup> consortium. The telescope is equipped with a new  $4k \times 4k$  CCD camera having a pixel scale of  $0''.289/\text{pixel}$ , which allows one to cover a field of  $20' \times 20'$ . This allows us to cover the entire cluster, which has an estimated diameter of 18 arcmin (Dias et al. 2002).

Observations were carried out on November 30, 2005. Three Landolt (1992) areas (TPhoenix, Rubin 149, and PG 0231+006) were also observed to calibrate the instrumental magnitudes to the standard system. The night was photometric with an average seeing of 1.1 arcsec. Data were reduced using IRAF<sup>2</sup> packages CCDRED, DAOPHOT, and PHOTCAL. Photometry was done employing the point spread function (PSF) method (Stetson 1987). The covered area is shown in Fig. 1, while Table 1 contains the observational log.

The calibration equations read:

<sup>1</sup> <http://www.astro.yale.edu/smarts/>

<sup>2</sup> IRAF is distributed by NOAO, which is operated by AURA under cooperative agreement with the NSF.

**Table 1.** Journal of photometric observations of NGC 2112 and standard star fields together with calibration coefficients (November 30, 2005).

Field	Filter	Exposure time [sec.]	Seeing	Airmass [ $\mu$ ]
NGC 2112	U	1200,60,5	1.1	1.150-1.280
	B	900,30,3	1.0	1.150-1.280
	V	600,30,1	1.0	1.150-1.280
	I	600,30,1	1.0	1.150-1.280
TPhoenix	U	180,200	1.0	1.024,1.444
	B	90,120	1.1	1.023,1.447
	V	20,30	1.1	1.024,1.450
	I	40,40	1.1	1.022,1.452
PG 0231+006	U	200,240	1.1	1.291,1.801
	B	60,90	1.1	1.293,1.807
	V	40,40	1.1	1.296,1.809
	I	40,30	1.1	1.294,1.810
Rubin 149	U	180,240	1.0	1.311,1.651
	B	90,120	1.1	1.316,1.649
	V	30,40	1.0	1.318,1.647
	I	40,40	1.0	1.313,1.643
Calibration coefficients	$u_1 = +3.285 \pm 0.004$			
	$u_2 = +0.032 \pm 0.006$			
	$u_3 = +0.46$			
	$b_1 = +2.188 \pm 0.004$			
	$b_2 = -0.160 \pm 0.006$			
	$b_3 = +0.27$			
	$v_{1bv} = +2.188 \pm 0.014$			
	$i_1 = +2.789 \pm 0.044$			
	$i_2 = +0.021 \pm 0.043$			
	$v_{2bv} = +0.017 \pm 0.018$			
	$i_3 = +0.06$			
	$v_3 = +0.12$			
	$v_{1vi} = +2.188 \pm 0.016$			
	$v_{2vi} = +0.013 \pm 0.016$			

$$u = U + u_1 + u_2(U - B) + u_3X \quad (1)$$

$$b = B + b_1 + b_2(B - V) + b_3X \quad (2)$$

$$v = V + v_{1bv} + v_{2bv}(B - V) + v_3X \quad (3)$$

$$v = V + v_{1vi} + v_{2vi}(V - I) + v_3X \quad (4)$$

$$i = I + i_1 + i_2(V - I) + i_3X \quad (5),$$

where  $UBVI$  are standard magnitudes,  $ubvi$  are the instrumental magnitudes,  $X$  is the airmass, and the derived coefficients are presented at the bottom of Table 1. To compute  $V$  magnitudes when  $B$  magnitudes were available, we used expression (3); otherwise we used expression (4). The standard stars in these fields provide a wide color coverage with  $-1.217 \leq (U - B) \leq 2.233$ ,  $-0.298 \leq (B - V) \leq 1.999$ , and  $-0.361 \leq (V - I) \leq 2.268$ . Aperture corrections were estimated in a sample of 15 bright stars and then applied to all stars. They amounted to 0.315, 0.300, 0.280, and 0.280 mag for the  $U$ ,  $B$ ,  $V$ , and  $I$  filters, respectively.

We cross-correlated our photometry with the photoelectric sequence of Richtler (1985) to check our zero-points. The cross-identifications are listed in Table 2, where for comparison purposes we approximate our values to two digits, as in R85. Values that have not been measured either by R85 or by us are replaced with 99.999.

The differences in  $V$ ,  $B - V$  and  $U - B$  between R85 and our study are illustrated in Fig. 2, and amount to:

$$\Delta V = 0.02 \pm 0.06,$$

$$\Delta(B - V) = 0.02 \pm 0.04, \text{ and}$$

$$\Delta(U - B) = -0.01 \pm 0.09$$

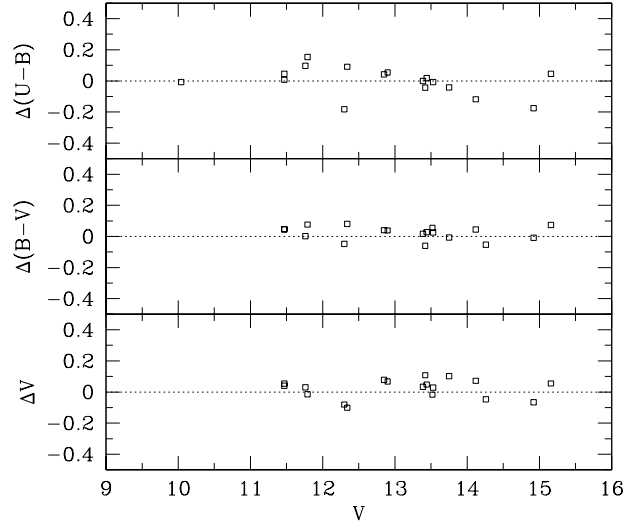


**Figure 2.** Comparison of our photometry with the Richtler(1985, R85) photoelectric sequence.

Our photometry is basically consistent with R85. Only  $U - B$ , although in agreement, exhibits a significant scatter.

The resulting CMDs are shown in Fig. 3 for three color combinations. The TO is located at  $V \sim 14.5$ ,  $(B - V) \sim 1.1$ , and  $(V - I) \sim 1.3$ .

## 2.2 Spectroscopy: HYDRA observations

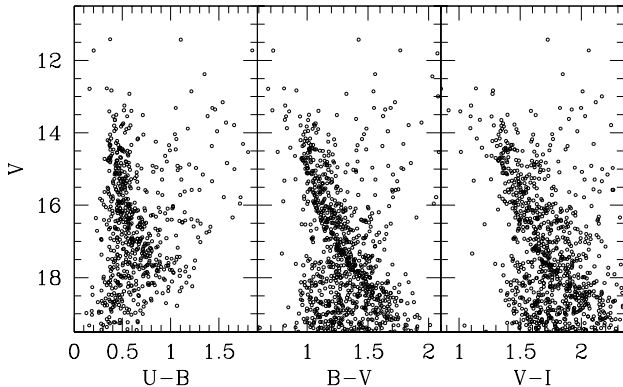
Medium resolution spectroscopic observations were carried out on the night of 2006 Feb 15 (Julian Date 2453783.57006) with the Hydra spectrograph on-board the Wisconsin Indiana Yale NOAO (WIYN) telescope at Kitt Peak National Observatory under photometric conditions and typical seeing of 1.0 arcsec. The Multi-Object Spectrograph (MOS) consists of the Hydra positioner, which in 20 minutes can place 89 fibers within the  $1^\circ$  diameter focal plane of the telescope to 0.2 arcsec precision. This project employed the 3 arcsec diameter red-optimized fiber bundle.

The fibers feed a bench-mounted spectrograph in a thermally isolated room. With the echelle grating and the Bench Spectrograph Camera, the system produces a resolution of 15000 at 6560 Å. The wavelength coverage of 400 Å around the central wavelength of 6560 Å provides a rich array of narrow absorption lines. We observed 35 TO-RGB stars with  $2 \times 45$  minute exposures, for a grand total of 1.5 hr of actual photon collection time on each star.

The 35 stars were selected from the photometric catalog presented in previous section. By using UCAC2 catalog (Zacharias et al 2004) as reference, we converted pixel coordinates into 2000.0 equinox Right Ascension and Declination using 50 stars as input. The astrometry precision is 0.3 arcsec. The selected stars for Hydra are candidate RGB and TO stars according to their position in the CMD and have the right magnitudes to be observed with the WIYN 3.6 m telescope. We restricted the sample to stars brighter than

**Table 2.** Comparison of the our photometry with the photoelectric sequence of Richtler(1985,R85)

$ID_{R85}$	$ID$	$V_{R85}$	$(B - V)_{R85}$	$(U - B)_{R85}$	$V$	$(B - V)$	$(U - B)$
1-01	630	11.47	0.58	0.38	11.42	0.54	0.37
1-02	593	13.53	1.04	0.43	13.50	1.02	0.43
1-06	585	11.76	0.72	0.30	11.73	0.72	0.20
1-10	512	13.44	1.12	0.61	13.39	1.09	0.59
1-16	382	10.04	2.25	2.62			2.62
1-18	401	14.92	0.99	0.52	14.99	0.99	0.70
2-02	601	13.75	1.00	0.38	13.65	1.01	0.42
2-16	422	13.39	1.66	1.46	13.36	1.64	1.46
2-20	724	12.85	0.85	0.38	12.77	0.81	0.34
3-03	749	12.90	0.95	0.44	12.83	0.91	0.39
3-06	909	15.16	1.11	0.47	15.11	1.04	0.42
3-08	919	14.26	1.74		14.31	1.79	1.75
3-09	1029	14.12	1.22	0.60	14.05	1.17	0.72
3-10	935	13.52	1.68		13.54	1.62	1.38
3-16	1123	12.34	2.11	2.77	12.44	2.03	2.68
3-17	1026	11.79	2.15	2.64	11.80	2.07	2.49
3-18	954	13.42	1.49	1.01	13.31	1.55	1.05
4-01	711	12.30	1.51	1.17	12.38	1.56	1.35
4-02	759	11.47	1.47	1.15	11.43	1.42	1.10

**Figure 3.** CMD for the stars in the field of NGC 2112 in the  $V$  vs  $U-B$  (left panel),  $V$  vs  $B-V$  (medium panel) and  $V$  vs  $V-I$  (right panel).

$V \sim 15.0$ . The stars are listed in Table 2, where column (1) reports numbering. In the following columns we report 2000.0 equinox coordinates, magnitude and colors, heliocentric radial velocity, and proper motion components from UCAC2 (Zacharias et al. 2004). In the last column an indication of membership is provided (see next section). For some stars (#782, 655, 890 and 417), no proper motions are available from UCAC2, probably because these stars have close companions.

Images were pre-reduced using IRAF<sup>3</sup> including bias subtraction, flat-field correction, frame combination, extraction of spectral orders, wavelength calibration, sky subtraction, and spectral normalization. Some spectra turned out to have a very low signal-to-noise ratio (S/N), although all the

**Table 4.** Observational details of the 5 stars observed with MIKE

ID	Julian Date	Exposure sec	S/N
535	2454303.82317	500	80
261	2454403.81600	800	60
717	2454403.83538	1200	100
304	2454403.85079	1600	90
836	2454403.87042	1300	80

observed stars have practically the same magnitude. This could happen for two reasons: the first is an imperfect pointing of the fiber, and the second is possibly bad fiber transmission.

### 2.3 Spectroscopy: MIKE observations

Echelle spectrograms of stars #535, #261, #717, #304 and #836 (see Table 2) were obtained on 2007 October 29 with the Magellan Inamori Kyocera Echelle (MIKE) spectrograph mounted on the Nasmyth focus of Landon Clay 6.5m telescope at the Magellan Observatory. Data were obtained with both the blue and red arms. The slit was 0.7 arcsec wide, which yielded a resolution  $R=33000$ , and the CCD was binned in steps of 2 pixels in the dispersion direction. The typical seeing was 0.6-0.8 arcsec. We used quartz lamp images without the diffuser in position for flat field correction, and the wavelength calibration was performed with ThAr lamp images that were taken just before and after the five stellar exposures. The dark current was checked by examining several dark exposures and was found to be insignificant. The optimum algorithm (Horne 1986) was used to extract the spectra, which were also sky-subtracted and normalized using IRAF routines. Additional details on the spectra are reported in Table 3.

<sup>3</sup> IRAF is distributed by the National Optical Astronomy Observatory, which is operated by the Association of Universities for Research in Astronomy, Inc., under cooperative agreement with the National Science Foundation.

The old open cluster NGC 2112: updated estimates of fundamental parameters based on a membership analysis This

**Table 3.** Basic properties of the stars for which we secured spectroscopic observations. In the last column, M indicates members according to radial velocity, NM indicates non-members

ID	RA <i>hh : mm : ss.s</i>	DEC <i>° : ' : ''</i>	U	B	V	$\sigma V$	I	RV <sub>H</sub> [ <i>km/sec</i> ]	$\mu_{\alpha} \cdot \cos \delta$ [ <i>mas/yr</i> ]	$\mu_{\delta}$ [ <i>mas/yr</i> ]	
HYDRA observations											
101	05:53:11.7	+00:18:43.4	17.409	15.983	14.363	0.017	12.476	42.47±0.68	3.6±7.9	-10.8±8.2	NM
124	05:53:13.2	+00:26:20.9	17.397	16.204	14.873	0.016	13.226	-3.16±0.78	2.7±8.1	-11.0±7.8	NM
167	05:53:16.0	+00:15:06.6	16.433	15.000	13.313	0.018	11.315	29.60±0.40	-3.6±7.9	8.8±7.8	M
185	05:53:17.1	+00:25:00.3	16.269	15.834	14.852	0.015	13.501	36.53±0.96	-3.6±7.8	-3.2±7.8	NM
244	05:53:22.1	+00:21:23.7	15.913	15.433	14.407	0.015	13.026	32.02±0.82	-2.4±7.9	-2.8±7.9	M
274	05:53:24.7	+00:27:19.5	16.907	16.094	14.909	0.016	13.247	-15.67±1.62	-3.5±7.8	4.2±7.9	NM
323	05:53:28.2	+00:25:09.8	16.715	16.057	14.896	0.016	13.305	30.69±1.90	-7.5±7.8	3.0±7.9	M
340	05:53:29.1	+00:29:37.5	16.264	15.418	14.246	0.016	12.655	32.27±0.74	-10.1±7.9	2.9±7.9	M
382	05:53:31.4	+00:27:18.7	14.876	12.249				-6.18±0.22	-1.2±1.0	-7.5±1.1	NM
399	05:53:32.4	+00:23:49.2	15.600	15.073	13.998	0.016	12.518	28.39±0.60	-0.3±7.8	5.5±7.8	M
417	05:53:33.3	+00:22:53.3	16.547	15.369	13.882	0.017	12.052	29.49±0.25			M
422	05:53:33.7	+00:17:42.9	16.461	15.000	13.357	0.018	11.435	-29.32±0.26	-6.3±7.8	-15.1±7.8	NM
443	05:53:34.8	+00:16:16.0	16.550	15.505	14.037	0.016	12.275	29.52±0.34	-5.9±7.8	4.1±7.9	M
478	05:53:37.0	+00:21:12.5	15.528	14.988	13.898	0.016	12.428	30.45±0.44	1.2±7.8	4.4±7.8	M
512	05:53:39.0	+00:27:50.7	15.077	14.485	13.392	0.019	11.805	21.42±1.52	-0.9±7.8	-7.9±7.8	NM
542	05:53:40.9	+00:18:17.1	15.307	14.820	13.824	0.015	12.458	30.78±0.54	-1.8±7.9	0.9±7.8	M
566	05:53:42.3	+00:24:46.2	16.006	15.561	14.539	0.015	13.141	30.03±0.67	-2.1±7.8	-2.8±7.9	M
577	05:53:42.7	+00:16:10.3	16.016	15.512	14.454	0.015	13.036	27.55±0.65	-2.1±7.9	5.1±8.0	NM
580	05:53:42.8	+00:29:55.3	15.317	14.807	13.739	0.016	12.380	-12.84±0.67	10.8±7.9	0.2±7.9	NM
593	05:53:43.7	+00:23:56.5	14.953	14.517	13.502	0.017	12.105	44.78±0.49	-15.3±7.8	-2.0±7.8	NM
601	05:53:44.4	+00:23:00.7	15.076	14.654	13.647	0.019	12.302	30.02±0.60	1.0±7.8	-5.4±7.8	M
655	05:53:47.3	+00:26:16.6	16.416	14.877	13.155	0.018	11.036	31.55±0.21			M
656	05:53:47.5	+00:22:01.6	15.337	13.491	11.724	0.019	9.663	29.53±0.27	3.2±1.7	-0.8±1.7	M
707	05:53:50.3	+00:25:22.1	15.495	15.148	14.202	0.015	12.900	30.81±0.81	-9.2±8.0	27.3±7.9	M
714	05:53:50.7	+00:23:18.7	15.672	15.226	14.227	0.015	12.843	31.95±0.70	1.9±7.8	1.1±7.9	M
737	05:53:51.9	+00:24:33.8	15.526	15.143	14.157	0.015	12.825	31.81±0.57	-1.7±7.8	-6.2±8.0	M
770	05:53:53.6	+00:18:56.4	16.235	15.794	14.767	0.015	13.379	24.37±0.86	1.7±7.8	-5.8±7.9	NM
782	05:53:54.3	+00:21:01.0	15.466	14.754	13.510	0.017	11.883	31.41±0.24			M
794	05:53:55.0	+00:24:08.0	15.727	15.293	14.280	0.015	12.884	20.71±0.57	3.0±7.8	5.5±8.1	NM
824	05:53:56.6	+00:25:24.8	15.698	15.327	14.366	0.015	13.056	30.65±0.58	-0.9±7.8	3.8±7.9	M
890	05:53:59.9	+00:23:12.4	15.393	15.019	14.051	0.015	12.728	12.00±0.53			NM
917	05:54:02.0	+00:24:56.4	16.075	15.724	14.757	0.016	13.436	22.70±1.16	-12.0±7.8	0.2±8.2	NM
935	05:54:03.1	+00:22:59.5	16.546	15.162	13.537	0.018	11.505	38.33±0.22	1.0±7.8	-4.3±7.8	NM
936	05:54:03.2	+00:24:16.8	15.987	15.671	14.719	0.015	13.384	-26.71±1.81	-12.9±7.8	4.2±7.8	NM
1140	05:54:22.6	+00:21:32.6		14.947	13.964	0.021	12.581	3.89±1.01	-1.0±7.8	3.3±7.9	NM
MIKE observations											
261	05:53:23.6	+00:15:35.9	17.100	15.619	13.955	0.015	11.987	19.84±0.14	-6.3±7.8	-6.7±7.9	NM
304	05:53:27.1	+00:23:33.3	16.059	15.402	14.181	0.015	12.583	29.27±0.15	-4.2±7.8	-0.6±7.9	M
535	05:53:40.6	+00:18:31.4	15.326	14.826	13.770	0.017	12.317	29.55±0.25	2.7±7.9	-1.9±7.9	M
717	05:53:50.9	+00:25:30.8	15.676	15.308	14.336	0.012	12.998	39.03±0.24	4.1±7.9	0.6±7.9	NM
836	05:53:57.3	+00:26:06.1	16.681	15.622	14.171	0.014	12.402	29.26±0.16	-6.1±8.1	3.2±7.9	M

**Table 5.** Radial velocity: comparison with literature data

R85	ID	V	(B-V)	RV <sub>H</sub>	BWGO96	FJ93	MM07
1-16	382			-6.18±0.22	-3.6		- 4.04
2-4	656	11.724	1.767	29.53±0.27	30.04		
2-16	422	13.357	1.643	-29.32±0.26	-23.3	-22	-29.02
3-16	1123	12.441	2.030			21	31.75
3-17	1026	11.805	2.073			40	44.76
3-18	954	13.312	1.550		25.3		
4-1	711	12.380	1.639				28.56
4-2	759	11.429	1.423		21.6÷30.1	35	32.53
4-16	883	12.856	1.546		44.5	60	

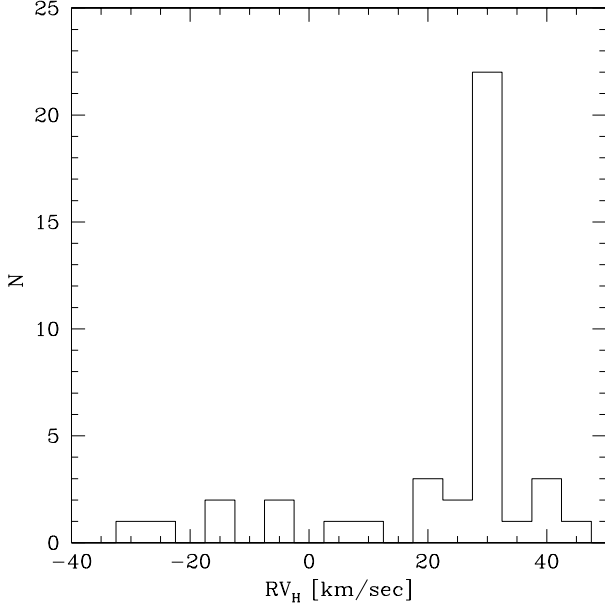


**Figure 4.** Distribution of radial velocities from the present study.

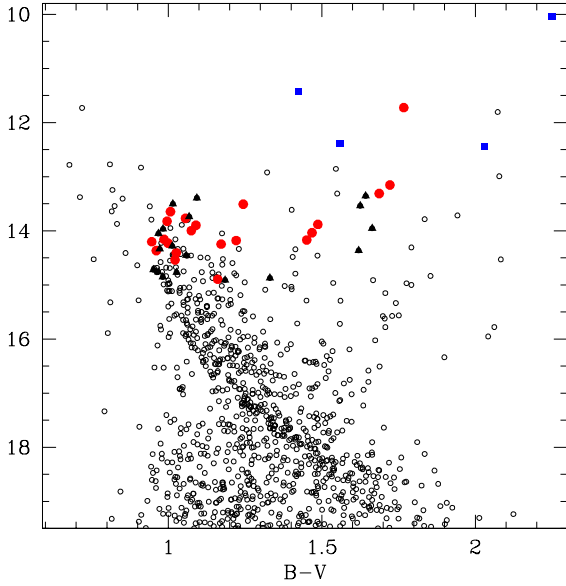


**Figure 5.** CMD of NGC 2112. Filled circles (red when printed in color) indicate radial velocity members, while filled triangles (black in color) non-members. Filled (color coded in blue) squares are member stars for which we do not have either photometry or radial velocity. See text for additional details.

### 3 MEMBERSHIP AND CLUSTER MEAN RADIAL VELOCITY

We derived radial velocities of the target stars using the IRAF *fxcor* task, which cross-correlates the object spectrum with a template. As a template, we used a synthetic spec-

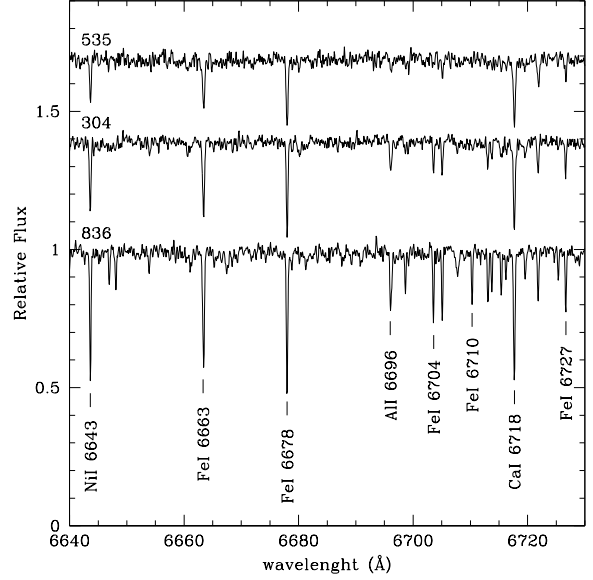


**Figure 6.** Extracted spectra for the 3 MIKE member stars. A few important lines are indicated

trum calculated by SPECTRUM<sup>4</sup> with roughly the same atmospheric parameters and metallicity of the observed stars. The final errors in the radial velocities, as provided by *fxcor*, were typically less than 1.0 km/s for most of the Hydra stars and less than 0.3 km/s for MIKE targets (see Table 2). In the case of Hydra spectra, these have to be considered the real errors since they have been taken from the average of the two different exposures and their combined errors. In the case of MIKE spectra, having only one exposure, we consider the reported error as a lower limit of the real error. The distribution of radial velocities is shown in the histogram in Fig. 4. The bulk of stars form a peak in the heliocentric radial velocity distribution around 30-31 km/s, allowing us to define a mean velocity for the cluster and the dispersion,  $\sigma$ . These turn out to be:

$$RV_H = 30.9 \pm 0.4 \text{ km/s} \quad (1)$$

To derive this value we used 21 stars, which are listed in Table 2 as cluster members. These stars were selected using an interactive procedure in which we calculated an initial value for  $RV_H$  and  $\sigma$ . Then stars having radial velocities more than  $3\sigma$  from the mean were rejected as non-members and a new  $RV_H$  and  $\sigma$  computed. This procedure was iterated until no more stars were rejected.

It is, however, possible that some of the rejected stars are binary stars.

In Table 4, we compare our measurements with literature values. Radial velocity data for NGC 2112 are poor and very inhomogeneous. We have 3 stars in common with BWGO96, one with FJ93 and 2 with MM07. In all cases, the radial velocities are compatible within the errors, as are

<sup>4</sup> SPECTRUM is the local thermodynamical equilibrium (LTE) spectral synthesis program freely distributed by Richard O. Gray. See: <http://www.phys.appstate.edu/spectrum/spectrum.html>

**Table 6.** Atmospheric parameters of MIKE member stars

ID	$T_{\text{eff}}(\text{K})$	$\log(g)$	$v_t(\text{km/s})$	$[\text{Fe}/\text{H}]$
535	6650	3.85	1.70	$0.15 \pm 0.02$
304	5980	3.65	1.00	$0.19 \pm 0.02$
836	5130	3.48	1.02	$0.13 \pm 0.01$

the membership assignments.

We confirm the result of BWGO96 that star #2-4 (our star 656) is a member.

One more star, for which we do not have new radial velocity, can be considered a member, following MM07, if it is a binary: this is star #3-18 (our 954).

Finally, we find that #3-16, 4-1 and 4-2 (our stars 1123, 711 and 759) are member stars following the analysis in MM07 and looking at Table 5.

We make use of the CMD to get additional information on the cluster membership. In Fig. 5, we indicate with filled circles (red when printed in color) the radial velocity members, and with filled triangles (black when printed in color) the radial velocity non-members. Additionally, we plot as filled squares (blue in color) stars that are members, but for which we do not have radial velocity measurements (1123, 711 and 759), and star 362 (#3-16), for which we have measured its radial velocity but not photometry, which we take from R85..

Clearly, members and non-members mix up in a way that, without radial velocities, it would not be possible to discriminate between them. Our member stars are partly located in the TO region and partly trace the sub-giant branch and RGB of the cluster.

Among this membership sample, we find two stars with the radial velocities typical of members but located far from the most important loci in the CMD. They are stars #323 at  $(V, B-V) = (14.896, 1.161)$  and #782 at  $(13.510, 1.244)$ . We suggest that these stars may be binary members, as is star #3-18 (our 954, see MM07), which must be confirmed by future studies (but see Section. 7 for additional details). Unfortunately, we cannot use proper motions (see Table 2) to improve our membership assignments due to the large associated errors.

## 4 ABUNDANCE MEASUREMENTS

### 4.1 Atomic Parameters and Equivalent Widths

We performed the analysis of chemical abundances on the 3 members observed with MIKE using the 2007 version of the free available program *MOOG* developed by Chris Sneden<sup>5</sup> and using model atmospheres by Kurucz (1992). *MOOG* performs a local thermodynamic equilibrium (LTE) analysis. We derived equivalent widths of spectral lines by Gaussian fitting of spectral features. Repeated measurements show a typical error of about 5 mÅ for the weakest lines. The line list was taken from Carraro et al. (2008). The  $\log(gf)$  parameters of these lines were re-determined by a solar-inverse analysis measuring the equivalent widths from the NOAO

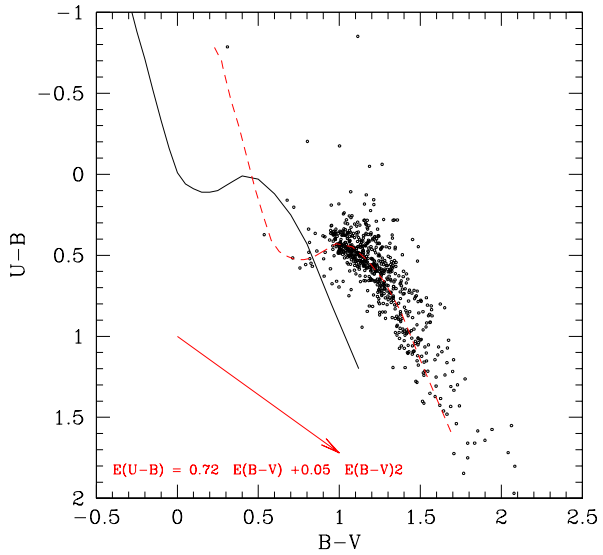


**Figure 7.** Two-color diagram for NGC 2112 stars. The solid line is the Schmidt-Kaler (1982) empirical ZAMS and the dashed line is the same ZAMS shifted by  $E(B-V)=0.60$  along the reddening vector (the arrow) for a normal reddening law.

solar spectrum (Kurucz et al. 1984), adopting standard solar parameters ( $T_{\text{eff}} = 5777 \text{ K}$ ,  $\log(g) = 4.44$ , and  $v_t = 0.8 \text{ km/s}$ ). The *O* abundance was obtained from the IR triplet at 7771-5 Å, while the Na abundance was obtained from the spectral doublets at 5662-68 and 6154-60 Å. These features are well known to be affected by NLTE effects. For this reason we applied NLTE correction to the output LTE abundances, obtained from Gratton & al. (1999).

### 4.2 Atmospheric Parameters

Initial estimates of the atmospheric parameter  $T_{\text{eff}}$  were obtained from photometric observations using the relations from Alonso et al. (1999). We adopted  $E(B-V)$  values from Carraro et al. (2002) to correct colours for interstellar extinction. We then adjusted the effective temperature by minimizing the slope of the abundances obtained from Fe I lines with respect to the excitation potential in the curve of growth analysis. Initial guesses for the gravity  $\log(g)$  were derived from the canonical formula:

$$\log \left( \frac{g}{g_{\odot}} \right) = \log \left( \frac{M}{M_{\odot}} \right) + 4 \log \left( \frac{T_{\text{eff}}}{T_{\odot}} \right) - \log \left( \frac{L}{L_{\odot}} \right) \quad (2)$$

In this equation, the mass  $M/M_{\odot}$  was derived from the comparison between the position of the star in the Hertzsprung-Russell diagram and the Padova isochrones (Girardi et al. 2000). The luminosity  $L/L_{\odot}$  was derived from the absolute magnitude  $M_V$ , assuming a distance moduli of  $(m - M)_V = 11.6$ . The bolometric correction (BC) was derived from the BC-Teff relation from Alonso et al. (1999). The input  $\log(g)$  values were then adjusted in order to satisfy the ionization equilibrium of Fe I and Fe II during the abundance analysis. Finally, the microturbulence velocity is given by the relation (Houdashelt et al. 2000):

<sup>5</sup> <http://verdi.as.utexas.edu/moog.html>

$$v_t = 2.22 - 0.322 \times \log(g) \quad (3)$$

We then adjusted the micro-turbulence velocity by minimizing the slope of the abundances obtained from Fe I lines with respect to the equivalent width in the curve of growth analysis. The adopted values for all these parameters, together with [Fe/H], are reported in Table 6. The results of the abundance analysis are listed in Table 7, where the abundances of the main elements are reported with their uncertainties. Two stars turn out to be giants (# 304 and 836), while star #535 is clearly a dwarf. This explains the different number of lines used in the determination of the different elemental abundances.

As a final remark, we also performed an abundance analysis for the two radial velocity non-members, and found that the two stars #261 and #717 have [Fe/H] =  $+0.28 \pm 0.02$  and  $+0.30 \pm 0.03$ , confirming their nature as non member stars.

Examples of our extracted spectra are illustrated in Fig. 6, in which the spectrum of 3 MIKE member stars are shown and some interesting lines indicated.

The mean metallicity we derive ([Fe/H]= $+0.16 \pm 0.03$ ) is significantly different from any previous spectroscopic estimate. The closest determination is the one by BWGO96, who found [Fe/H]= $-0.15 \pm 0.15$ . Our result rules out any possibility that NGC 2112 is very metal poor, as suggested in early studies. It would have been very unusual to have such a metal poor cluster in the solar neighborhood. Our result, in fact, suggests that NGC 2112 has a typical solar vicinity metal abundance, being as metal rich as the Hyades (Boesgaard & Friel 1990).

Karatas & Schuster (2006) provided a new calibration of the relation between the metallicity of a dwarf star and  $\delta_{0.6}$ , namely the (U-B) excess/deficiency with respect to the Haydes sequence at (B-V) $_o = 0.6$ . We compared the distribution of dwarf stars in NGC 2112 at (B-V) $_o \sim 0.6$  with respect to a ZAMS from Girardi et al. (2002) having the same metallicity of the Hyades ([Fe/H]=0.17). We found that the useful stars (13 in number) have  $\delta_{0.6} = -0.02 \pm 0.11$ . Despite the scatter, this  $\delta_{0.6}$  implies a metallicity close to our spectroscopic determination (see Table 3).

## 5 ABUNDANCE RATIOS

We derived abundance ratios for the 3 MIKE member stars listed in Table 7. Previously, only BWGO96 provided an estimate of a few abundance ratios in NGC 2112, but based on just one star. At any rate, we compare our findings with BWGO96 (their Table 6), and find basic agreement with [O/Fe] and [Na/Fe]. However, their [Al/Fe] is much larger than our value.

Being close to the Sun and having roughly the same metallicity, it is useful to make a detailed comparison of the chemical properties of NGC 2112 with the solar neighborhood stars and star clusters.

### 5.1 Comparison with field stars

Bensby et al. (2005) present a detailed abundance analysis for a sample of 102 F and G dwarf stars in the solar vicinity.

#### $\alpha$ -elements

As shown by Bensby et al (2005), *O*, *Mg*, *Si*, *Ca* and *Ti* exhibit similar trends in the Galactic thin disk. At the Fe abundance of NGC 2112 ( $+0.16$ ), these ratios are in the range of  $-0.15:0.00$ ,  $0.00:0.15$ ,  $0.00:0.15$ ,  $0.00:0.15$ , and  $-0.05:0.05$  dex, respectively.

According to our findings, abundance ratios for these five elements in NGC 2112 are in agreement with the thin disk values within the errors. This confirms that NGC 2112 is a typical thin disk star cluster. The overall  $[\alpha/\text{Fe}]$  ratio turns out to be  $0.04 \pm 0.03$ .

#### Iron peak elements

We can compare only *Ni* and *Cr* with Bensby et al (2005). *Ni* is basically in agreement with the thin disk trends, whereas the [Cr/Fe] ratio is marginally overabundant.

#### Al and Na

While the *Na* abundance relative to *Fe* is consistent with thin disk values, we find that Al is significantly under-abundant.

#### r- and s-process elements

We measured *Y* and *Ba* abundance ratios. While the *Ba* abundance in NGC 2112 is consistent with the thin disk trend, we find that the *Y* abundance is significantly larger than typical thin disk values.

### 5.2 Comparison with open clusters

In general, there is not much information on abundance ratios in open clusters, and only in the last few years efforts have been done to improve this situation.

Here, we compare our NGC 2112 abundance ratios with the results presented in Friel et al. (2003). They provide a detailed abundance analysis of the old star cluster Collinder 261 and compare its abundance ratios with a sample of 10 open clusters (see their Table 7). From this table, we extract estimates for NGC 2360 and NGC 6819, two nearby clusters having roughly the same ages and metal abundances as NGC 2112. We find that within the errors, NGC 2360 and NGC 6819 possess the same  $[\alpha/\text{Fe}]$  as NGC 2112,  $+0.03$  and  $0.00$ , respectively.

The *Na* abundance of NGC 2112 is similar to NGC 2360 but significantly lower than in NGC 6819. As for *Al*, we can make a comparison only with NGC 6819, for which [Al/Fe] is similar to the value we determine for NGC 2112.

Unfortunately, neither information about the Iron-peak elements nor for s- and r- process elements are reported in Friel et al. (2003).

Overall, with a few exceptions, we find that NGC 2112 is a genuine thin disk population cluster.



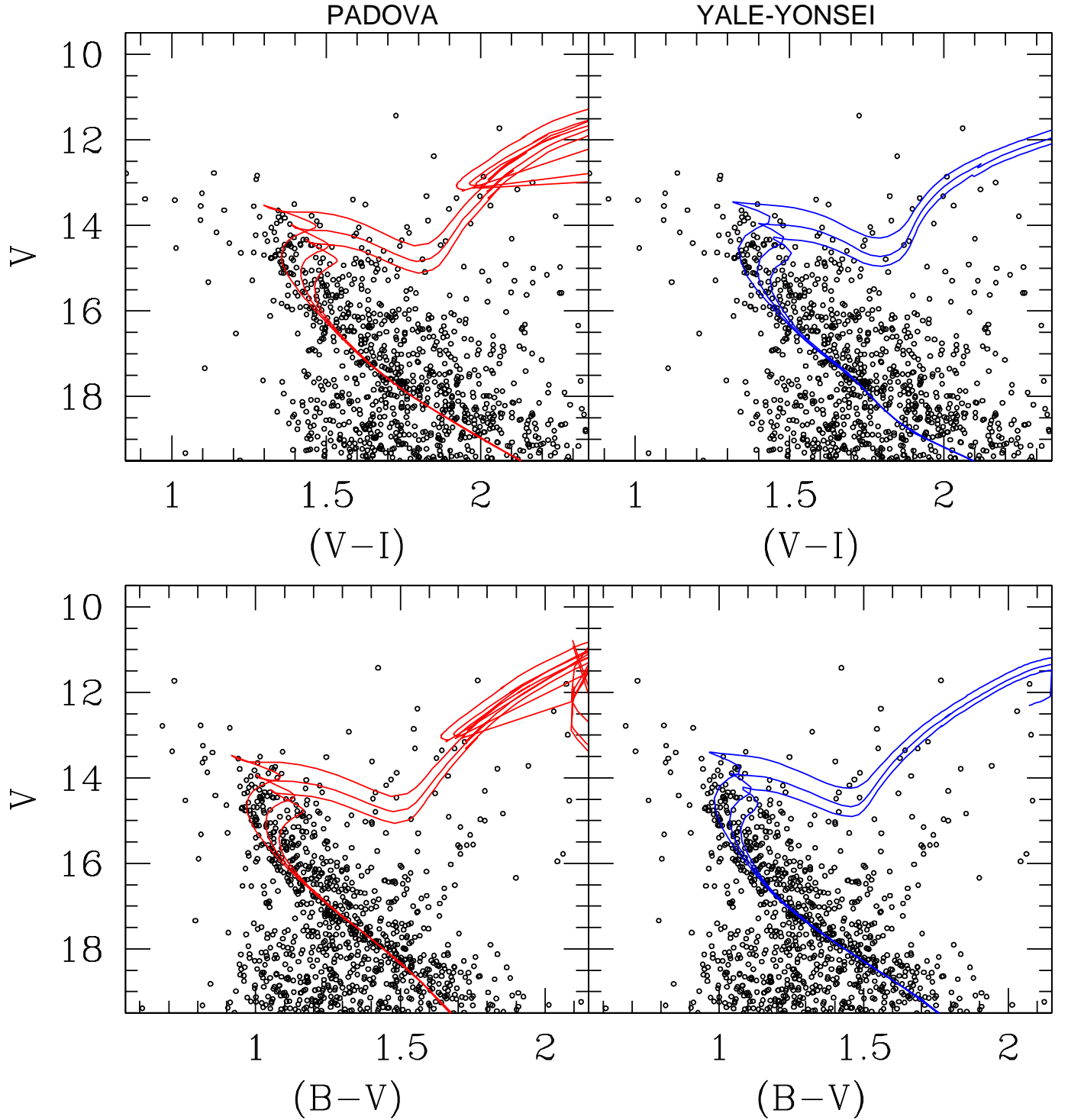


**Figure 8.** Isochrone fits for the derived metallicity and varying ages. Bottom panels show the fits in the  $V$  vs  $(B-V)$  plane, upper panels in the  $V$  vs  $(V-I)$  planes. Left panel refers to Padova isochrones, and right panels to Yale-Yonsei isochrones.

## 6 CLUSTER FUNDAMENTAL PARAMETERS

Having an estimate of the metal content ( $[\text{Fe}/\text{H}] = +0.16$ ), and of the  $\alpha$ -element abundances ( $[\alpha/\text{Fe}] = +0.04$ ), we are now in the position to derive more reliable estimates of the

cluster parameters.

The reddening value in the direction of NGC 2112 predicted by Schlegel et al. (1998) maps is  $E(B-V) = 1.01$ . This has to be considered as an upper limit to the reddening since it takes into account the absorption all the way to infinity.

**Table 7.** Abundance analysis from MIKE cluster members. After each value, in parenthesis, the number of lines  $N$  used is indicated. Values derived from just one line do not have any error associated.

<i>Element</i>	#535	$N$	#304	$N$	#836	$N$
[Fe/H]	0.15±0.02	(19)	0.19±0.02	(71)	0.13±0.01	(107)
[O/H] <sub>LTE</sub>	0.45±0.07	(3)	0.36±0.01	(3)	0.27±0.03	(3)
[O/H] <sub>NLTE</sub>	0.03±0.07	(3)	0.17±0.01	(3)	0.23±0.03	(3)
[Na/H] <sub>LTE</sub>	0.35±0.13	(2)	0.20±0.06	(4)	0.30±0.06	(3)
[Na/H] <sub>NLTE</sub>	0.24±0.13	(2)	0.15±0.06	(4)	0.23±0.06	(3)
[Mg/H]	0.13	(1)	0.18	(1)	0.27±0.03	(2)
[Al/H]			0.10±0.09	(2)	0.05±0.03	(3)
[Si/H]	0.33±0.02	(3)	0.11±0.06	(5)	0.11±0.05	(8)
[Ca/H]	0.18±0.07	(7)	0.23±0.04	(13)	0.07±0.05	(13)
[Ti/H]	0.20±0.04	(2)	0.43±0.09	(7)	0.23±0.04	(23)
[V/H]			-0.01	(1)	0.31±0.06	(10)
[Cr/H]	0.51±0.05	(2)	0.41±0.08	(6)	0.14±0.03	(11)
[Mn/H]	-0.18	(1)	0.03±0.03	(3)	0.10±0.02	(3)
[Co/H]			0.27±0.07	(2)	0.24±0.06	(4)
[Ni/H]	0.17	(1)	0.24±0.05	(15)	0.21±0.03	(29)
[Cu/H]			0.38	(1)	0.12	(1)
[Y/H]			0.45	(1)	0.51±0.24	(2)
[Ba/H]	0.59	(1)	0.84±0.06	(2)	0.40±0.01	(2)

To get an independent estimate of the reddening in the direction of NGC 2112, we make use of the two-color diagram (TCD) in Fig. 7 since we provide deep  $U$  band photometry for the first time. Here, the solid line is the zero reddening empirical Zero Age Main Sequence (ZAMS) from Schmidt-Kaler (1982). The same ZAMS, shifted by  $E(B-V)=0.60$  is shown as a dashed line. The shift has been performed adopting the standard reddening law (see the expression in the bottom of Fig. 7), and the reddening vector is indicated with a solid arrow.

We compare the distribution of stars in the various color combination CMDs and sets of theoretical Padova (Girardi et al. 2000) and Yale (Demarque et al. 2004, Kim et al. 2002, Yi et al 2001) isochrones. The physical ingredients of the two sets, and the possible sources of different results, have been discussed exhaustively in Carraro et al. (2006), where a similar exercise has been done for the very metal rich open cluster NGC 6791.

In Fig. 8 we superimpose isochrones with  $[Fe/H]=+0.16$  and  $[\alpha/Fe]=+0.04$  for 3 ages (1.5, 2.0, and 2.5 Gyrs). The fitting is performed in the left panels for Padova models, and in the right panels for Yale models.

To derive more constrained basic parameters, we consider in Fig. 9 the star distribution in the  $V$  vs  $(B-V)$  plane, and we highlight the radial velocity members using filled circles. The best fit isochrone is found for an age of  $1.8\pm0.3$  Gyr, where the associate error has been derived by trying different age isochrones.

We find that the both the Yale-Yonsei and Padova sets fit the star distribution well, and we summarize the derived values for the basic parameters in Table 8.

On average, we obtained  $(m-M)_V=11.75\pm0.15$  and  $E(B-V)=0.60\pm0.10$ . The errors here reported have been derived by displacing the best fit isochrone back and forth in the distance modulus and reddening directions and exploring the values of distance modulus and reddening which produce acceptable fits.

The two sets of models imply the same values for NGC 2112 basic parameters within the errors. It is worth

**Table 8.** Abundance ratios from MIKE cluster members

<i>Element</i>	#535	#304	#836
[O/Fe] <sub>NLTE</sub>	-0.12	-0.02	0.10
[Na/Fe] <sub>NLTE</sub>	0.09	-0.04	0.10
[Mg/Fe]	-0.02	-0.01	0.14
[Al/Fe]		-0.09	-0.08
[Si/Fe]	0.18	-0.08	-0.02
[Ca/Fe]	0.03	0.04	-0.06
[Ti/Fe]	0.05	0.24	0.10
[V/Fe]		-0.20	0.18
[Cr/Fe]	0.36	0.22	0.01
[Mn/Fe]	-0.33	-0.16	-0.03
[Co/Fe]		0.08	0.11
[Ni/Fe]	0.02	0.05	0.08
[Cu/Fe]		0.19	-0.01
[Y/Fe]		0.26	0.38
[Ba/Fe]	0.44	0.65	0.27

**Table 9.** Summary of NGC 2112 fundamental parameters derived from the comparison of different isochrone sets.

Models	Age	$E(B-V)$	$(m-M)_V$
Yale-Yonsei	$1.8\pm0.3$	$0.63\pm0.05$	$11.80\pm0.10$
Padova	$1.8\pm0.3$	$0.57\pm0.05$	$11.75\pm0.10$

noticing, however, that the fit implies a sizeable difference in the mean  $E(B-V)$ , in the sense that the reddening that inferred using Yale-Yonsei models is larger than that inferred from Padova models. At the same age and metal abundance, the apparent Yale-Yonsei RGB is bluer than the Padova one, resulting in a larger reddening when fitting the observed RGB.

Using the heliocentric rectangular Galactic coordinates  $X=9.3$  kpc,  $Y=-400$  pc, and  $Z=-200$  pc and assuming the Sun distance from the Galactic center is 8.5 kpc, NGC 2112 is located  $940\pm70$  pc from the Sun towards the anti-center direction. Consequently, we infer a distance of 9.3 kpc from the Galactic center.

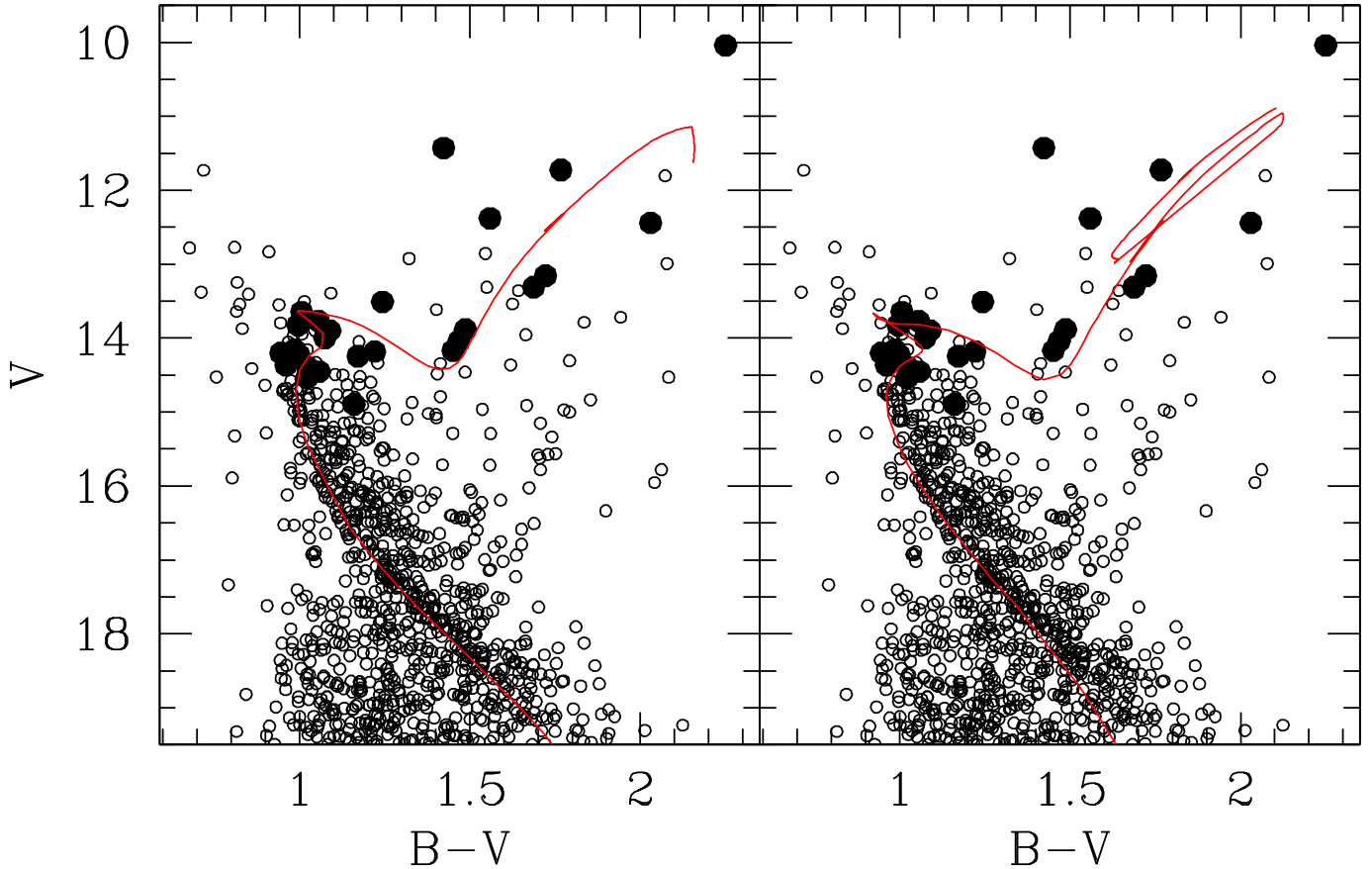


**Figure 9.** The best fit isochrone is super-imposed on the NGC 2112 CMD where radial velocity members are indicated with solid circles. Left panel refers to Yale-Yonsei isochrones, and the right panel to Padova isochrones. The isochrones have been adjusted using the values listed in Table 8.

## 7 A ZOOM OF THE TO REGION: GETTING ADDITIONAL CLUES TO THE BINARY POPULATION

Now that we have determined the cluster’s fundamental parameters, we can use the best fit isochrone as a tool to investigate possible binaries among cluster members from a purely photometric point of view. In Fig 10 we provide a zoom of the TO region, and indicated with filled circles (color coded in red) radial velocity members. The solid line is the best fit Padova isochrone (see Fig. 9). The dashed curve is the same isochrone, but shifted up by 0.75 mag, to illustrate the locus of unresolved equal mass binaries. This exercise is suggesting us that several stars that lie off the best fit isochrone may in reality be unresolved binaries. In fact some of them lie very close to the binary locus, and we indicate them as filled squares (color coded in green) in the CMD of Fig. 10. They are stars #707, 824, 782 and 601. At the same time, we indicated as filled triangles (blue when printed in color) stars which lie neither in the single star nor in the binary star sequence. These are stars #714, 707, and 323. One may speculate that these are unequal mass binaries or maybe systems with more than two components. If we refer only to the TO region, we are left with 14 single

member stars and 7 possibly multiple systems, which implies a rough binary percentage of 33%.

## 8 DISCUSSION AND CONCLUSIONS

In this paper we presented new photometric and spectroscopic data in the field of the old open cluster NGC 2112. This new dataset allowed us to revise the cluster’s fundamental parameters and clarify a long lasting debate on its properties, which for many years have been poorly constrained due to the high level of field star contamination. By means of multi-fiber spectroscopy, we measured radial velocity for 40 stars and found 21 radial velocity members. This, in turn, allowed us to clean the CMD, providing a better comparison with stellar models.

The most important result of our study is that the cluster has a metallicity much higher than previous determinations, and somewhat higher than the Sun. Also the  $\alpha$ -elements are marginally enhanced with respect to the Sun, but still compatible with the trends of thin disk stars in the solar vicinity, as are all the other elements we measured. Therefore NGC 2112 is typical of old, thin disk star clusters,

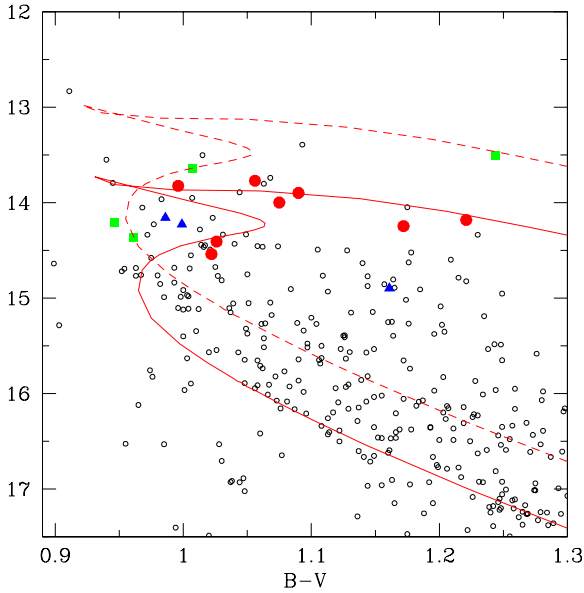


**Figure 10.** A zoom of the TO region in NGC 2112 CMD. Filled circles indicate *bona fide* single stars, filled squares possible equal mass binary systems, and filled triangles multiple systems or unequal mass binaries. The solid line is the best fit isochrone which is also shown in Fig. 9, whereas the dashed line is the same isochrone shifted upward by 0.75 mag. to mimic the location of equal mass binaries.

as metal rich as the Hyades (Boesgaard & Friel 1990), and located at less than 1 kpc from the Sun in the anticenter direction.

In addition, we confirmed the age of the cluster ( $\sim 1.8$  Gyr), previously derived on a purely photometric basis (Carraro et al. 2002). As for the distance and reddening, our values are in agreement within the errors of previous determinations.

This study stresses the importance of performing detailed membership analysis in Galactic open clusters in order to derive more robust estimates of their fundamental parameters.

## ACKNOWLEDGMENTS

This research was part of a joint project between Universidad the Chile and Yale University, partially funded by the Fundación Andes. Hydra observations were performed remotely from Yale by MVM. CMB acknowledges Universidad de Chile graduate fellowship support from program MECE Educación Superior UCH0118 and Fundación Andes C-13798. MVM was supported by an NSF Astronomy and Astrophysics Postdoctoral Fellowship, under award AST04-011640. GC thanks Doug Geisler, Tom Richtler and Roberto Barbon for long and interesting discussions on NGC 2112, and the anonymous referee who helped us to improve the paper presentation. This study made use of SIMBAD and WEBDA.

## REFERENCES

- Alonso, A., Arribas, S. & Martínez-Roger, C. 1999, A&AS, 140, 261
- Bensby, T., Feltzing, S., Lundström, I., Ilyin, I., 2005, A&A 433, 185
- Boesgaard, A.M., Friel, E.D., 1990, ApJ 351, 467
- Brown J.A., Wallerstein G., Geisler D., & Oke J. B. 1996, AJ, 112, 1551
- Carraro, G., Ng, Y.K., & Portinari, L. 1998, MNRAS, 296, 1045
- Carraro, G., Barbon, R., & Boschetti, C.S. 2002, MNRAS, 336, 259
- Carraro G., Villanova, S., Demarque, P., McSwain, M.V., Piotto, G., Bedin, L.R., 2006, ApJ 643, 1151
- Carraro G., Geisler, D., Villanova, S., Frinchaboy, P.M., Majewski, S.R., 2008, A&A 476, 217
- Demarque P., Wo, Y.-H., Kim, Y.-C., Yi, S.K. 2004, ApJS 115, 667
- Dias, W.S., Alessi, B.S., Moitinho, A., Lepine, J.R.D. 2002, A&A 389, 871
- Friel E.D., Janes K.A., 1993, A&A 267, 75
- Friel, E.D., Jacobson, H.R., Barrett, E., Fullton, L., Balachandran, S.C., Pilachowski, C.A, 2003, AJ 126, 2372
- Geisler D. 1987, AJ, 94, 84
- Geisler D., Claria J.J., Minniti, D. 1991, AJ, 102, 1836
- Girardi L., Bressan A., Bertelli G., & Chiosi, C. 2000, A&AS, 141, 371
- Gratton R. G., Carretta E., Eriksson K., & Gustafsson B. 1999, A&A, 350, 955
- Houdashelt M.L., Bell R.A., & Sweigart A.V. 2000, AJ, 119, 1448
- Horne, K., 1986, PASP 98, 60
- Karatas Y., Schuster W.J., 2006, MNRAS 371, 1793
- Kim, Y.-C., Demarque, P., Alexander, D.R., 2002, ApJS 143, 499
- Kurucz R.L., Furenlid I., Brault J., & Testerman, Larry 1984, sfat.book, K
- Kurucz R.L. 1992, IAUS, 149, 225
- Janes, K.A., Phelps, R.L., 1994, AJ 108, 1773
- Landolt, A.U., 1992, AJ 104, 340
- Mermilliod, J.-C., Mayor, M., 2007, A&A 470, 919
- Richtler T. 1985, A&AS, 59, 491
- Richtler T., & Kaluzny J. 1989, A&AS, 81, 225
- Schlegel D.J., Finkbeiner D.P., & Davis M. 1998, ApJ, 500, 525
- Schmidt-Kaler, Th., 1982, in Schaifers K., Voigt, H.H., eds., Numerical Data and Functional Relationships in Science and Technology, Landolt-Börnstein, New Series, Group VI, Vol 2(b), Springer, Berlin, p. 14
- Stetson, P.B., 1987, PASP 99, 191
- Zacharias, N., Urban, S.E., Zacharias, M.I., Wycoff, G.L., Hall, D.M., Monet, D.G., Rafferty, T.J., 2004, AJ 127, 3043
- Yi, S.K, Demarque P., Kim, Y.-C., Lee, Y.-W., Ree, C.H., Lejeune, Th., Barnes, S., 2001, ApJS 136, 417